Turkish Journal of Physics

Volume 22 | Number 9 Article 5

1-1-1998

A Study of Heavy-Ion Elastic Scattering Reactions Using a Semimicroscopic Model

A. A. FARRA

Tr. J. of Physics
22 (1998) , 895 – 900.

A Study of Heavy-Ion Elastic Scattering Reactions Using a Semimicroscopic Model

A. A. FARRA
Physics Department, Faculty of Science
Al-Azhar University, Gaza - PALISTINE

Received 14.01.1998

Abstract

The differential cross sections for elastic scattering of ^{16}O from ^{20}Ne have been calculated using an optical potential and distorted wave Born approximation (DWBA) calculations. In the present calculations several prescriptions were tried in the ion-ion potential. The DWBA calculations were performed employing folded real and Woods-Saxon optical potentials for the distorted waves. Inclusion of the exchange process explains the large back-angle cross sections. The elastic scattering differential cross sections are successfully described by calculations in which elastic alpha-transfer amplitudes are coherently added to direct elastic scattering amplitudes.

1. Introduction

Heavy ion elastic scattering data have been studied successfully in terms of a double-folding potential [1, 2]. The use of folded optical potentials for the distorted waves has been introduced in an analysis of single-nucleon transfer reaction [3]. The elastic scattering angular distributions [4] have been analyzed over the large angular range using woods-Saxon potential. The contribution of parity-dependent real potential was found in the analysis of heavy ion elastic scattering data [5]. The differential cross sections for elastic scattering of ^{28}Si from ^{27}Al have been analyzed in terms of the optical Potential with a Woods-Saxon form factor and the phase shift model [6]. Several description have been developed to describe the gross structures observed in $^{16}O+$ ^{20}Ne elastic scattering [7-9].

In the present work, a microscopic $^{16}O +$ ^{20}Ne interaction potential has been constructed in a double-folding model with M3Y interaction and a single-nucleon exchange term. The elastic transfer process was calculated as an alpha-particle transfer in the DWBA calculations. Section 2 describes the reaction amplitude. Numerical calculations and results are given in Section 3. Section 4 contains the discussion and conclusion.

2. Reaction Amplitude

In an attempt to find a more consistent analysis of the data in the whole angular range, the elastic transfer amplitude was calculated as an α-cluster transfer in the exact finite-range DWBA calculations.

In the present section, we used the explicit transfer amplitude which has been introduced in previous calculations [10],

$$T_{tr}(M_A, \pi - \theta) = S(2J_a + 1)^{1/2} \sum_{\ell} (2\ell + 1)^{1/2} \langle J_A M_A | J_A M_A \rangle F_{\ell m}(\pi - \theta), \qquad (1)$$

where J_A and M_A are the spin and spin component of target nucleus A; S is the specteoscopic factor for the $\alpha - {}^{16}O$ substructure of ${}^{20}Ne$; and ℓ is the orbital momentum transferred in the $A(a, A)a$ reaction. In the present calculations, the from factor $F_{\ell m}$ has been calculated following the analysis of heavy ion transfer reactions [11]. The calculated α-elastic transfer amplitude was added coherently to the direct amplitude T_{el} describing the $A(a, a)A$ scattering process. Dealing with the coherent sum of the two channel components, the transition amplitude for the spin-zero colliding particles can be expressed as

$$T_{sys}(\theta) = T_{el}(\theta) + T_{tr}(\pi - \theta). \qquad (2)$$

The direct elastic amplitude have been calculated using an optical model. Where in the absence of any spin-orbit interaction it is independent of spin component and behaves as a term with transferred angular momentum $\ell = 0$.

3. Numerical Calculations and Results

In the present calculations, different interpretations are introduced to explain the elastic scattering data. Initially, the data have been analyzed using the standard six-parameter Woods-Saxon potentials. The starting parameters were varied to give the best fit to the 24.5 MeV data. The resulting parameters are given in Table 1. In addition, an optical model using real and imaginary double-folding potentials [12] was employed. In this analysis, the effective nucleon-nucleon interaction is taken to be the $S = T = 0$ components of the $M3Y$ interaction [13]. In the present calculations the folding potential was carried out using the $DFPOT$ [14] version of computer program. Where a harmonic oscillator distribution and a two-parameter Fermi density were used to construct the density distributions of ${}^{16}O$ and ${}^{20}Ne$ nuclei, respectively. Listed in Table 2 are the parameters of these distributions which are obtained from electron scattering measurements [15], assuming that the proton and neutron densities to be identical. In these calculations, there are a fewer adjustable parameters because the densities of the nuclei considered are obtained independently. The real N_R- and imaginary N_1-normalization factors were varied until the best fit to the data was obtained. The results are given in Table 3 and the fits shown as a dotted line in Figure 2. It is seen that the normalization coefficient of the real part is larger than unity and larger than the coefficient of the imaginary part. In fact, using the same folded form for both real and imaginary ($DF + DF$)

potentials does not fit the data. Therefore, the conventional Woods-Saxon shape was used for the imaginary part of the optical potential together with the usual Coulomb potential. In this analysis the folded potential was multiplied by a normalization factor N to compensate for deficiencies in the model. Initially, the normalization factor was fixed at $N = 1.0$ and the imaginary potential parameters were extensively searched upon to fit the data. In a second set of calculations, searches were done on the imaginary parameters over a gird of N values in steps of 0.1. The parameters obtained are listed in Table 3 and the fits shown in Figs. 1 and 2 as a dashed lines. It is apparent that the fits to the 32.1 MeV data are good over the entire angular range and provide a much better description of the data than that using $(DF + DF)$ potentials. In order to describe the experimental data in the whole angular range, the differential cross sections have been evaluated using the DWBA calculations. The numerical calculations have been carried out using the SATURN-MARS versions of computer program [16]. In the present calculations, the binding potentials is taken as a Woods-Saxon potential with parameters $r_0 = 1.25fm$ and $a_0 = 0.65fm$. The strength was adjusted to give the single particle separation energies and the number of nodes for the wave function were calculated using the harmonic oscillator relation. In general, the data have been described qualitatively in terms of the interference of elastic α-transfer amplitudes with the elastic scattering amplitudes as shown in Figures 1 and 2 as a solid lines.

Table 1. Optical model potentials for the $^{16}O + {}^{20}Ne$ elastic scattering

E		V_0	r_v	a_v	W_0	r_w	a_w
(MeV)	Set	(MeV)	(fm)	(fm)	(MeV)	(fm)	(fm)
24.5	I	10.0	1.48	0.45	23.0	1.32	0.35
32.1	II	25.0	1.42	0.51	9.6	1.25	0.29
	III	44.0	1.34	0.59	15.0	1.19	0.35

$$V_{opt} = V_c - V_0 f(X_V) - W f(X_W); f(X_i) = \left\{1 + \exp\left(\frac{r - R_i}{a_i}\right)\right\}^{-1}$$

$R_X = r_X(A_1^{1/3} + A_2^{1/3}); \quad x = v,\ w$ and c.

Table 2. Charge density parameters

Nucleus	ρ_o (fm^{-3})	a (fm)	c (fm)	α_0
^{16}O	0.07256	1.818		1.529
^{20}Ne	0.07675	0.571	2.805	

$$\rho_c(r) = \rho_0[1 + \alpha_0(r/a)^2]\exp[-(r/a)^2] \quad \text{for} \quad {}^{16}O.$$
$$= \rho_0[1 + \exp[(r - c)/a]^{-1} \quad \text{for} \quad {}^{20}Ne.$$

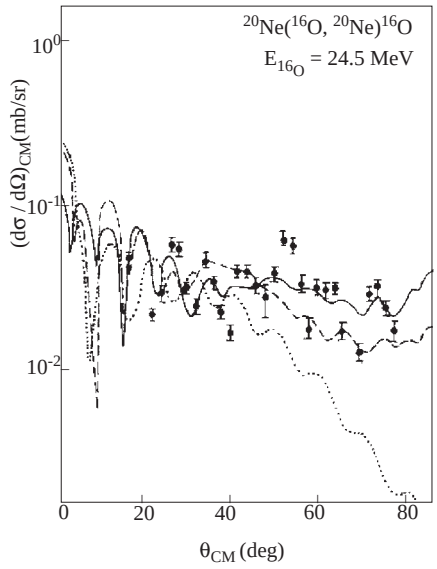

Figure 1. The differential cross sections for the $^{20}Ne(\ ^{16}O,\ ^{20}Ne)\ ^{16}O(g.s.)$ reactions. The solid curve is the coherent sum of direct elastic-and elastic transfer-components. The dashed line is the result of DF+WS optical model calculations. The dotted line is the DF+DF analysis. The experimental data are from reference [7].

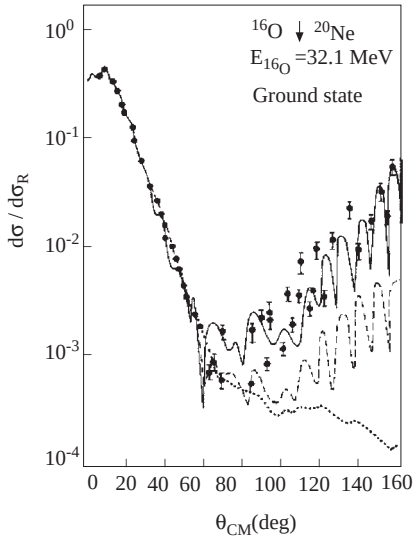

Figure 2. As in Fig. 1. The experimental data are from reference [7].

4. Discussion and Conclusion

In the present work, the $^{16}O+\ ^{20}Ne$ elastic scattering data were analyzed in terms of different optical models. The present calculations show that the backward oscillations for the 32.1 MeV elastic scattering data can't be described in terms of the folding-model. In fact, the folding potential provides reasonably good fits to the experimental data as well as the Woods-Saxon potential. The most obvious difference between the double folding predictions and the phenomenological fits are in the cross sections at the backangles. The DF calculations fit the data fairly well and then fall off precipitously, whereas the optical potential calculations show a rising backangle cross sections. Also, the results obtained with using a semimicroscopic analysis are in good agreement with the experimental data as shown in Figs. 1 and 2 by dashed lines. It is found that different normalization factors together with different families of discrete ambiguous potentials introduce good fits to the data and give qualitatively similar results as those obtained in the previous calculations [7] using an extended optical model.

Table 3. Best fit parameters of folding model

System	E (MeV)	N_R	N_I	N	W_0 (MeV)	r_w (fm)	a_w (fm)
$^{16}O+\ ^{20}Ne$	24.5	1.0			16.0	1.49	0.31
		1.23	0.73				
				0.79	16.0	1.41	0.28
	32.1	1.0			7.6	1.35	0.27
		1.39	0.69				
				0.74	23.0	1.13	0.39

In addition, it is seen that calculations using a coherent sum of the direct elastic amplitudes and elastic transfer amplitudes introduce the best fits to the elastic data in the complete angular range as shown in Figs. 1 and 2 as a solid lines. Where the present calculations provide a substantially better description of the elastic scattering angular distribution data than the coupled-channel calculations [9] using both a parity-dependent real interaction and an angular momentum-dependent absorbtive term. Therefore, the inclusion of the exchange process in the reaction amplitude well reproduces the phase and amplitude of the backward oscillations as well as the absolute value of the cross sections. It should be noted that although the one-step transfer process was responsible for the large angle cross sections, but it is insufficient to explain the $^{16}O+\ ^{20}Ne$ data in whole angular range. Moreover, the present analysis using the coherent sum of the two reaction amplitudes represent a significant improvement over the previous optical model calculations.

References

[1] B. Bilwes, R. Bilwes, L. Stuttge, F. Ballester, J. Diaze, J.L. Ferrero, C. Roldan and F. Sanchez, Nucl. Phys., **A473**, (1987) 353.

[2] M.El-Azab Farid and G.R. Satchler, Nucl. Phys. **A441** (1985) 157.

[3] C.W. Glover, K.W. Kemper and A.D. Frawley, Phys. Rev., **C22**, (1980) 522.

[4] M.F. Vineyard, J. Cook, K.W. Kemper and M.N. Stephens, Phys. Rev., **C30** (1984) 916.

[5] J.L. Ferrero, J.A. Ruiz, B. Bilwes and R. Bilwes, Nucl. Phys. **A510**, (1990) 360.

[6] S.K. Charagi, S.K. Gupta, M.G. Betigeri, C.V. Fernandes and Kuldeep, Phys. Rev., **C48**, (1993) 1152.

[7] Y. Kondo, B.A. Robson and R. Smith, Nucl. Phys. **A410**, (1983) 289.

[8] B.A. Robson and R. Smith, Phys. Lett., **B123** (1983) 160.

[9] Y. Kondo, B.A. Robson and R. Smith, Nucl. Phys. **A437** (1985) 117.

[10] W. von Oertzen and H.G. Bohlen, Phys. Rep. **C19** (1975) 1.

[11] K.S. Iow and T. Tamura, Phys. Rep. **C11** (1975) 789.

[12] G.R. Satchler and W.G. Love, Phys. Rep. **55** (1979) 183.

[13] G. Bretsch, J. Borysowicz, H.McManus and W.G. Love, Nucl. Phys., **A284** (1977) 399.

[14] J. Cook, Comput. Phys. Commun., **25** (1982) 125.

[15] C.W. De Jager and H.De Vries and C.De Vries, Nucl. Data Tables, **14**, (1974) 479.

[16] T. Tamura, T. Udagawa, K.W. Wood and H. Amakawa, Comput. Phys. Commun. **18** (1979) 163.